C. Arndt, W. Meier

Influence of Boundary Conditions on the Flame Stabilization Mechanism and on Transient Auto-Ignition in the DLR Jet-in-Hot-Coflow Burner

Flow, Turbulence and Combustion 102(4) (2019) 973-993.

http://dx.doi.org/10.1007/s10494-018-9991-6

Influence of Boundary Conditions on the Flame Stabilization Mechanism and on Transient Auto-Ignition in the DLR Jet-in-Hot-Coflow Burner

Christoph M. Arndt*, Wolfgang Meier

German Aerospace Center (DLR), Institute of Combustion Technology,

Pfaffenwaldring 38-40, D-70569 Stuttgart, Germany

*christoph.arndt@dlr.de

ORCID:

Christoph Arndt: 0000-0003-0871-6620

Wolfgang Meier: 0000-0002-1752-1246

Abstract

Transient auto-ignition is a key factor for flame stabilization and flame initialization in several technical combustion systems such as internal combustion engines or gas turbine combustors. Reliable numerical simulations of auto-ignition stabilized flames are important for the development of new combustor systems. For detailed model validation, knowledge of the sensitivity of different system response quantities (SRQs) of interest to the boundary conditions in combination with the accuracy of boundary conditions is essential, especially with respect to uncertainty quantification of numerical simulations. In the current study, the flame stabilization and auto-ignition in the DLR Jet-in-Hot-Coflow burner was examined experimentally using high-speed OH* chemiluminescence. Here, methane was either injected continuously to study the flame stabilization mechanism of steady state lifted jet flames, or in a pulsed manner to study the formation of auto-ignition kernels, into the hot exhaust gas of a lean, premixed hydrogen/air flame. The flame stabilization height, and the location and time of initial auto-ignition kernels for a case with transient auto-ignition were evaluated with respect to several boundary conditions, such as coflow temperature as well as coflow- and jet-velocity. A relative sensitivity of the measured SRQs on the boundary conditions was introduced in order to quantitatively compare steady state flame to transient auto-ignition characteristics and to assess the quantitative influence of different boundary conditions. Comparison of the auto-ignition dynamics in the steady state and during transient fuel injection allowed assessing the role of auto-ignition in the flame stabilization mechanism for different boundary conditions; accompanying chemical kinetic calculations were used to quantify the influence of strain on auto-ignition and flame propagation for the current conditions, allowing further insight into the flame stabilization mechanism in Jet-in-Hot-Coflow flames.

Keywords

Auto-Ignition; Jet-in-Hot-Coflow; Boundary Conditions; Flame Stabilization; Uncertainty Quantification

1 Introduction

Transient auto-ignition plays an important role in several technical combustion systems, such as internal combustion engines under Diesel or homogeneous compression charge ignition (HCCI) conditions, or gas turbine combustors. For the latter, especially in reheat combustors [1-3] or combustors with high levels of exhaust gas recirculation, such as FLOX® [4,5], or swirl combustors [5,6], auto-ignition can contribute to the flame stabilization process. In premixing sections, auto-ignition has to be avoided in order to prevent heat release in unwanted regions to avoid increased pollutant emissions or system damage [2,3].

For the study of flame stabilization and auto-ignition in systems where (cold) fuel is injected into a hot, oxygen-containing environment, Jet-in-Hot-Coflow (JHC) burners provide an excellent configuration. The flame stabilization [7-19], and to some extent also the influence of boundary conditions on the flame stabilization in JHC burners [14-19], have been described in the literature. Cabra et al. [14] reported an increasing lift-off height with increasing coflow- and jet velocity, while the lift-off height decreased with increasing coflow temperature. Similarly, Oldenhof et al. [15,20] found that in the Delft Jet-in-Hot Coflow burner, the lift-off height decreased with increasing coflow-temperature. When changing the jet velocity, the lift-off height decreased with increasing jet velocity for $Re < 5000$ due to a positive temperature gradient of the coflow and hotter coflow fluid being entrained at higher jet velocities. In contrast, for $Re > 5000$, the lift-off height increased with increasing Reynolds number due to room air being entrained at larger jet Reynolds numbers.

The transient formation of auto-ignition kernels in Jet-in-Hot-Coflow flames has also been studied in the literature [11,12,17,21-27]. For example, Gordon et al. [10] used planar imaging of temperature, CH_2O, and OH to examine the structure of individual ignition kernels upstream of stably burning flames resulting from natural gas issuing into a vitiated coflow. The imaging results indicated isolated ignition kernels, inferred from temperature and CH_2O increases, which were not always accompanied by OH and which occurred in regions of low-temperature gradients, indicating auto-ignition (and not flame propagation) was a primary mechanism governing the lifted flame stabilization. Similarly, Arndt et al. observed ignition kernels below the flame base for certain coflow temperatures, while for higher

coflow temperatures no ignition kernels were observed, suggesting auto-ignition is not the dominant flame stabilization mechanism for all operating conditions [17]. However, detailed studies on the influence of boundary conditions on the formation of ignition kernels and steady-state jet flames as well as flame stabilization mechanism regimes are sparse in the literature. Similarly, numerical simulations of JHC configurations focused on the steady-state flame stabilization [7,28-35]. Significant contributions to the understanding of the formation process of auto-ignition kernels have been made with direct numerical simulations (DNS) in 2D mixing layers [28]. However, full 3D simulations with appropriate models for transient kernel formation processes (such as large eddy simulation (LES)) are sparse in the literature. Here, especially data on the influence of different boundary conditions on the auto-ignition process is needed as validation data in order to assess simulation uncertainties and the quality of predictions by numerical simulations.

The current paper focuses on the influence of boundary conditions on the flame stabilization mechanism and on transient auto-ignition in the DLR Jet-in-Hot-Coflow burner (DLR JHC). While the formation of ignition kernels below a steady state lifted flame base in JHC configurations was reported and studied in the literature for certain ranges of coflow conditions [11,13,15,17,25], this effect is not visible for a broad range of operating conditions, especially for higher coflow temperatures [17]. Here, a lifted jet flame, which apparently stabilizes via flame propagation and not via auto-ignition is formed [17]. For the study of auto-ignition under those conditions, a transient fuel injection is mandatory. Furthermore, comparing the auto-ignition characteristics in the steady state and transient case allows the assessment of the contribution of auto-ignition on the flame stabilization mechanism in Jet-in-Hot-Coflow flames. Accompanying chemical kinetic calculations were performed in order to quantify the influence of strain on auto-ignition and flame propagation and to identify the most prominent flame stabilization mechanism (auto-ignition vs. flame propagation) for different boundary conditions.

Several boundary conditions, namely coflow and jet velocity, as well as the coflow temperature, were varied over a broad range and their influence on flame stabilization and transient auto-ignition was quantified. For steady state conditions, the flame lift-off height was used as system response quantity (SRQ) [36]. For the transient auto-ignition, the height and time of the first established auto-ignition

kernel served as SRQs. Several hundred auto-ignition events and long time-series of the steady state jet flame were measured via high-speed OH* chemiluminescence in order to gain sufficient statistical information. For a better comparison between different boundary conditions on flame stabilization and auto-ignition, a relative sensitivity is introduced as quantitative measure. Here, the relative change in the observed quantity (flame lift-off height, or auto-ignition height and time respectively) is put into relation to the relative change of the boundary condition, allowing the identification of the boundary condition where small changes have the largest impact. Especially for transient auto-ignition processes with temperatures and gas compositions corresponding to gas turbine application, such data is not available in the literature. Also, a quantitative comparison of the influence on flame stabilization versus auto-ignition is possible with this metric.

2 Experimental

2.1 DLR Jet-in-Hot-Coflow Burner (DLR JHC)

Details of the DLR JHC, schematically shown in Fig.1, have been described previously in the literature [11,17,21,24], so only the key features are presented here.

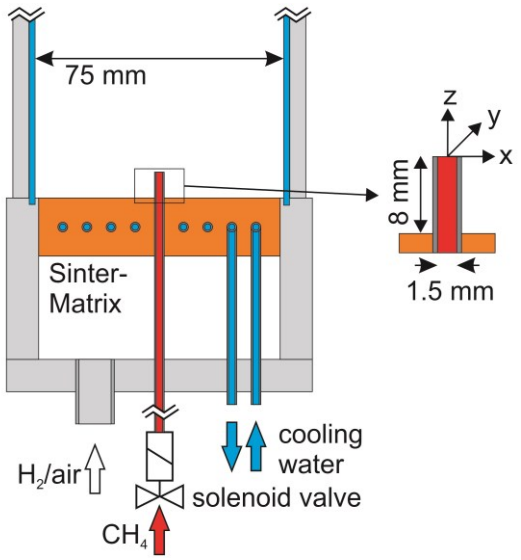

Figure 1. Schematic of the DLR Jet-in-Hot-Coflow Burner.

The hot coflow was generated by a lean premixed hydrogen/air flat flame that was stabilized on a water-cooled sintered bronze matrix with a cross section of 75 x 75 mm^2. The flame was confined by four quartz windows to prevent disturbance by ambient air. The nozzle was a stainless steel tube (inner diameter D = 1.5 mm), the tip of the nozzle was 8 mm above the matrix. Methane was either injected continuously for the study of lifted jet flames or in a transient manner for the study of auto-ignition kernels. For the transient fuel injection, a 2/2 way solenoid valve (Staiger VA204-5), located approximately 250 mm (or 165 D) below the nozzle exit (to ensure fully developed pipe flow), was used. The corresponding stagnation pressures in front of the solenoid valve for the different operating conditions studied here are listed in Table 3.

Since the tip of the fuel nozzle is in contact with the hot coflow, a slight preheat of the fuel could in principle occur. However, since for steady state case the residence time of the fuel in that part of the nozzle is extremely small (<< 1 ms) and, for the transient case, the volume of the fuel stagnant in the

nozzle during fuel injections is very small (and auto-ignition occurs away from the jet tip, where fuel preheating would be expected), this effect is considered negligible.

The operating conditions for the variation of the coflow temperature are summarized in Table 1 along with adiabatic equilibrium temperature (T_{ad}), measured coflow temperature (T_{cf}) and species mole-fractions for the coflow gases.

	Mass Flows / g/min				Coflow Composition			
φ	$\dot{m}_{H_2}$	$\dot{m}_{air}$	T_{ad} / K	T_{cf} / K	X_{N_2}	X_{H_2O}	X_{O_2}	ξ_{st}
0.440	3.80	300	1510	1450	0.7152	0.1688	0.1074	0.0311
0.465	3.86	285	1564	1501	0.7116	0.1778	0.1019	0.0297
0.485	3.90	276	1607	1543	0.7091	0.1844	0.0979	0.0286
0.506	3.95	268	1651	1585	0.7062	0.1915	0.0935	0.0275
0.527	3.99	260	1695	1627	0.7034	0.1986	0.0891	0.0263
0.548	4.03	253	1737	1668	0.7006	0.2057	0.0848	0.0252
0.567	4.07	246	1774	1703	0.6981	0.2119	0.0809	0.0241
0.586	4.10	241	1811	1739	0.6956	0.2182	0.0770	0.0231
0.607	4.17	236	1851	1777	0.6928	0.2250	0.0728	0.0219

Table 1. Operating conditions for the coflow for a coflow velocity of 4.1 m/s. T_{ad} is the adiabatic flame temperature, T_{cf} is the actual coflow temperature at z = 20 mm, based on Rayleigh measurements [21,24]. The coflow composition was calculated in the adiabatic equilibrium for a fresh gas temperature of 290 K using Gaseq [37]. ξ_{st} is the stoichiometric mixture fraction for the coflow-methane-mixtures.

The flow rates were controlled with Brooks MFC5850 mass flow controllers and monitored with coriolis flow meters (Siemens Sietrans Mass 2100) with an accuracy better than 1.5% [21]. Previous measurements have shown that the exhaust gas temperature stays very close to T_{ad} if heat loss to the matrix is minimized [21,24,38]. To meet this criterion the velocities of the unreacted gas were chosen to exceed 0.7 m/s. The actual coflow temperature was measured with laser Rayleigh scattering and was approximately 4% below T_{ad} [24], confirming the minimal heat loss.

In addition to the coflow temperature, the coflow velocity was chosen as a variable parameter. Table 2 summarizes the operating conditions for the studied coflow velocities for T_{cf} = 1585 K.

v_{cf} [m/s]	v_{cold} [m/s]	$\dot{m}_{H_2}$ [g/min]	$\dot{m}_{air}$ [g/min]	Re_{cf} [-]
3.6	0.70	3.51	238	4,800
4.1	0.79	3.95	268	5,500
5.0	0.97	4.87	330	6,700
5.9	1.14	5.71	387	7,900
6.8	1.32	6.59	447	9,100

Table 2. Operating conditions for different coflow velocities for an equivalence ratio of ϕ = 0.506. v_{cf} is the velocity of the hot coflow, calculated from the mass flows and the coflow temperature. v_{cold} is the fresh gas velocity calculated from the mass flows. $\dot{m}_{H_2}$ and $\dot{m}_{air}$ are the mass flows for hydrogen and air, Re_{cf} is the Reynolds number of the coflow.

Furthermore, the jet exit velocity v_{jet} was varied in the range of 92 m/s < v_{jet} <272 m/s, the operating conditions for the fuel jet are summarized in Table 3.

$\dot{m}_{CH_4}$ [g/min]	v_{jet} [m/s]	Re_{jet} [-]	p_{CH_4} [bar]
6.3	92	8,000	0.4
9.3	135	11,800	0.6
12.5	182	15,900	0.8
15.6	227	19,800	1.2
18.7	272	23,700	1.5

Table 3. Operating conditions for the fuel jet. $\dot{m}_{CH_4}$ is the fuel mass flow, v_{jet} is the jet exit velocity based on the fuel mass flow. Re_{jet} is the jet Reynolds number, p_{CH_4} is the static pressure in front of the solenoid valve (with pulsed fuel injection).

A coriolis meter in line with the CH_4-injection system was used to calculate the bulk flow velocity and jet exit Reynolds number. For the transient fuel injection, the jet exit velocity corresponds to the jet velocity (based on the bulk flow velocity calculated from the mass flow rates) after the jet switched from transient mode to steady state mode. The transition from a transient jet to a steady state jet occurs 1 – 2 ms after the jet exited the fuel nozzle [24]. Thus, the fuel jet is in the steady state (with constant fuel flow rate) before the onset of auto-ignition.

Before the measurements, the matrix burner was run for several minutes to achieve thermal equilibrium. For the steady state measurements, fuel was supplied using a mass flow meter, as mentioned above. Afterwards, a trigger started the camera recordings. A total of >15,000 frames per run condition were recorded in the steady state to get sufficient data for converged statistics. For the transient fuel injection, a trigger started the opening of the solenoid valve and the camera recording. The solenoid valve was opened for 50 ms, which is more than sufficient for the transient formation of ignition kernels (t > 10 ms) and the establishment of a steady state jet flame (t > 20 ms). The transient fuel injection was repeated 75 times at a rate of 0.5 Hz, corresponding to at least 60 times the coflow advection time (v_{cf} / combustion chamber height). This enabled the flow-field to regain a stationary state without the jet in between runs. After 75 recording cycles the images were downloaded from the cameras to a data acquisition computer and the sequence was repeated two times per operating condition, resulting in 225 individual transient injection/auto-ignition cases.

2.2 High Speed Imaging of OH* Chemiluminescence (CL)

Imaging of OH* CL was performed using an intensified high-speed CMOS camera (LaVision HSS8 with LaVision HS-IRO), equipped with a high-throughput UV lens (Cerco 45 mm, f/1.8, set to f/4) and a high-transmission bandpass filter (> 80% transmission at 310 nm). The frame rate was 20 kHz, the intensifier gate was 25 µs. For the stationary case, more than 15,000 image frames per run condition were recorded, for the transient auto-ignition, 225 individual ignition events, consisting of 250 frames each were recorded.

2.3 Data Analysis

The data analysis for the chemiluminescence measurements was described in [11,24], so only the key elements are described here. After darkfield and whitefield correction, the chemiluminescence images were smoothed with a 5 x 5 pixel median filter. After that, a 3 x 3 pixel software binning was applied to increase the signal-to-noise ratio, resulting in a spatial resolution of 0.3 mm. Single background photons being amplified by the image intensifier can lead to areas of several pixels with high signal intensities. In order to remove such image areas with high intensities, an additional filter was implemented. First, the images were converted from greyscale to black and white using an appropriate threshold. After thresholding the image, reacting regions were identified based on a size filter with a minimal area of 30 pixels. Every region smaller than 30 pixels was considered as noise and removed from the image. Therefore it was possible to distinguish reliably between ignition kernels and image intensifier noise with high intensities. The final image allowed the identification of reacting and non-reacting regions. A typical single shot of OH^* chemiluminescence for the steady state jet flame after image processing is shown in Figure 2.

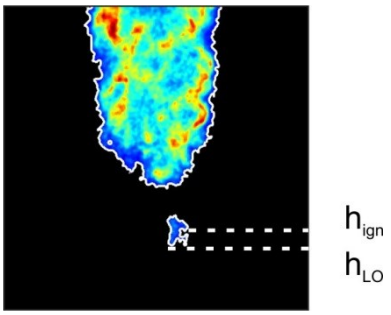

Figure 2. Typical OH chemiluminescence image of the steady state jet flame after image processing. The colour scale represents the OH* CL signal intensity, the white line corresponds to the reaction zone contour.*

Here, definitions of the lift-off height h_{LO} and of the ignition height are indicated by dashed white lines. The identified reaction zone contour is shown as solid white line. The lift-off height was defined as the lowest axial position of the reacting region for each image. The ignition height was the centroid of the first detected ignition kernel. The ignition time was the time when the first auto-ignition kernel was detected, with the jet tip exiting the fuel nozzle as reference time. The transient development of the fuel jet for determining the reference time for the ignition time was studied previously with laser Rayleigh scattering [24] and OH PLIF [39], depending on the experimental setup, since Rayleigh measurements are not available for all operating conditions. The reference time could be determined precisely with either technique and both techniques were validated with respect to each other. Furthermore, the temporal development of the transient fuel injection was very reproducible. A detailed discussion on measurement errors and uncertainties can be found in [11,24,17,39] and the key figures are summarized below.

Uncertainties in the measurement mainly stem from effects due to a finite temporal resolution when studying auto-ignition (which affects only the transient case). With an exposure time of 25 µs for each CL camera, and a velocities ranging between 4.1 m/s (coflow velocity) and 182 m/s (jet exit velocity for the reference test case), a maximum image slip of 4.5 mm is expected in the chemiluminescence imaging. However, since auto-ignition occurs at the outmost periphery of the jet, where the velocities are dominated by the coflow velocity, this effect was found to be approximately 0.1 mm/frame and thus negligible. The uncertainty of the ignition time is coupled to the uncertainty of the reference time of the jet exiting the fuel nozzle, which was found to be on the order of 0.05 ms [24].

2.4 Definition of System Response Quantities and Relative Sensitivities

To compare the influence of the variation of different boundary conditions BC on the system response quantities SRQ, a relative sensitivity s is defined:

$$s_{SRQ,BC} = \frac{\delta SRQ/\overline{SRQ}}{\delta BC/\overline{BC}}. \quad (1)$$

Here, the relative change of a system response quantity is compared to the relative change of a boundary condition, corresponding to the ratio of the change of the measurement quantity (in percent) relative to the change of the boundary condition (in percent). For SRQs which have a linear dependence to a given boundary condition, δSRQ and δBC (and $\overline{SRQ}$ and $\overline{BC}$) are calculated for the minimum and maximum values of the SRQ and the boundary condition respectively. For boundary conditions, which show a non-linear dependence (here the coflow temperature T_{cf}), δSRQ and δBC as well as the corresponding mean values are calculated for two adjacent data points, as stated below, where applicable. Thus, the relative sensitivity is suitable for comparing the influence of several boundary conditions on the same SRQ. While this metric relies on a single value and is self-referencing, it provides the clearest insight into the relative change of an SRQ, and also a good comparison of the behavior of different SRQs to the same boundary condition. However, for a better comparison of the absolute change of different SRQs to the same boundary condition, sometimes the knowledge of absolute dependencies is desirable, thus an absolute sensitivity S is defined:

$$S_{SRQ,BC} = \frac{\delta SRQ}{\delta BC}. \quad (2)$$

The absolute sensitivity provides a measure of the (absolute) change of an SRQ in response to the (absolute) change of a boundary condition. Since not all boundary conditions lead to a linear response of the SRQs (especially true for a change of the coflow temperature, as discussed in the following sections), a range of absolute and relative sensitivities is provided in case of non-linear response, allowing a comparison in certain temperature ranges.

2.5 Chemical Kinetic Modelling

Chemical kinetic calculations were performed in order to assess the extinction strain rate and the influence of strain on the flame speed for the current conditions. The extinction strain rates for the boundary conditions of the current experiment were calculated in a counterflow simulation using Cantera [40] and the method of Fiala and Sattelmayer [41] in conjunction with the GRI 3.0 reaction mechanism [42].

The influence of strain and scalar dissipation rate on auto-ignition was assessed in a previous study [17], using the software INSFLA [43]. Here, the dependence of the ignition delay time on the local strain rate was determined, as well as the critical strain rate k_{crit}, above which no auto-ignition can occur.

3 Results and Discussions

3.1 Influence of Boundary Conditions on the Steady State Jet Flame

First, the influence of different boundary conditions (coflow temperature, coflow and jet velocity) on the steady state jet flame will be discussed to get an overview of the flame behavior for different operating conditions. To demonstrate the dynamics of the steady state jet flame, Figure 3 shows a time series of OH^* chemiluminescence. For a space-saving presentation, only every third image frame is shown.

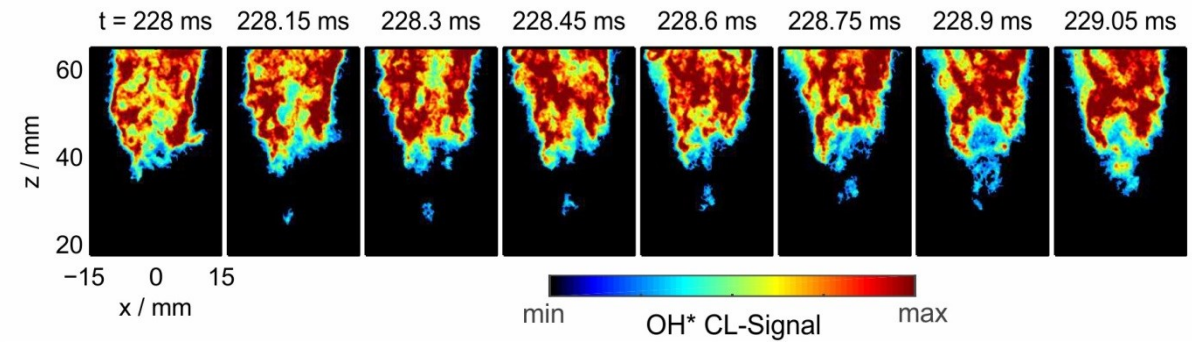

Figure 3. Time series of OH^* chemiluminescence for the steady state lifted jet flame for T_{cf} = 1501 K, v_{cf} = 4.1 m/s and v_{jet} = 182 m/s. For a space-saving presentation, every third image frame is shown.

At t = 228.15 ms, an ignition kernel is forming below the flame base which merges with the flame base at t = 228.9 ms. This behavior has been frequently observed, especially at the lower coflow temperatures studied here.

Figure 4 shows the influence of the coflow temperature T_{cf} on flame lift-off height h_{LO}. The symbols represent the average lift-off height $\bar{h}_{LO}$ (based on averaging the instantaneous lift-off height of >15,000 single OH* CL frames), the error bars represent the standard deviation ($\sigma_{h_{LO}}$) and the grey shaded area represents the range of measurement values. The blue line is a polynomial fit through the data points. Here, the coflow and jet exit velocity are kept constant at v_{cf} = 4.1 m/s and v_{jet} = 182 m/s, respectively. T_{cf} is controlled by changing the coflow equivalence ratio ϕ_{cf}. Thus, not only T_{cf} is changed, but also the coflow composition (oxygen, nitrogen, water and radicals). However, since the reaction rates (and hence the ignition delay time) are linearly dependent on composition and exponentially dependent on temperature, this is considered negligible here.

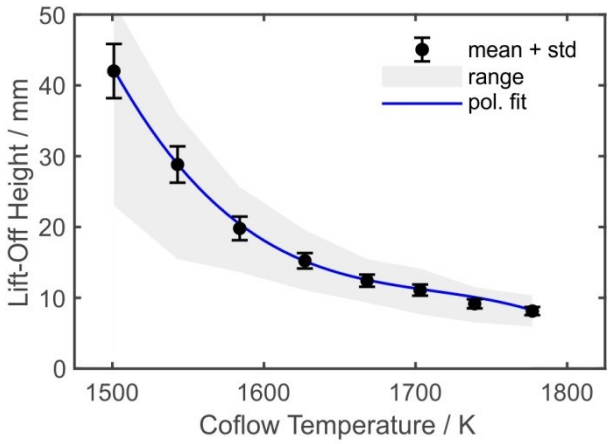

Figure 4. Dependence of the lift-off height on the coflow temperature. The black closed symbols correspond to the mean lift-off height, the error bars correspond to the standard deviation. The grey shaded area corresponds to the range of measured lift-off heights. The blue curve corresponds to a third-order polynomial fit and serves as guide to the eye.

With increasing T_{cf}, h_{LO} decreases significantly. This trend is non-linear and becomes less pronounced at higher T_{cf}. Consequently, the absolute and relative sensitivity (as described in Sec. 2.4) are not constant. For 1501 K < T_{cf} < 1541 K, the absolute sensitivity is $S_{\bar{h}_{LO},T_{cf}}$ = 0.38 mm/K; for 1668 K < T_{cf} < 1777 K, the absolute sensitivity decreases to $S_{\bar{h}_{LO},T_{cf}}$ = 0.05 mm/K. For 1501 K < T_{cf} < 1543 K the relative sensitivity is $s_{\bar{h}_{LO},T_{cf}}$ = 13.5 and for 1703 K < T_{cf} < 1739 K, it is $s_{\bar{h}_{LO},T_{cf}}$ = 3.0. The observed sensitivity of the flame lift-off height to the jet exit velocity is similar to the findings reported by Cabra et al. [14].

Since a change of the coflow velocity v_{cf} by a factor of two did not have a significant effect on h_{LO}, those results are not discussed here.

The dependence of the lift-off height h_{LO} of the steady-state jet flame on the jet exit velocity v_{jet} (and coupled the jet Reynolds number) is shown in Figure 5. The lift-off height $\bar{h}_{LO}$ scales linearly with v_{jet}: increasing v_{jet} by 1 m/s leads to an increase of $\bar{h}_{LO}$ of 0.13 mm ($S_{\bar{h}_{LO},v_{jet}}$ = 0.13 mm / m/s). The relative sensitivity of $\bar{h}_{LO}$ to a change of v_{jet} is $s_{(h_{LO},v_{jet})}$ = 1.15. Similarly, the standard deviation of the lift-off height, $\sigma_{h_{LO}}$, increases with increasing jet exit velocity and ranges from $\sigma_{h_{LO}}$ = 0.7 mm for v_{jet} = 92 m/s to $\sigma_{h_{LO}}$ = 3.2 mm for v_{jet} = 272 m/s.

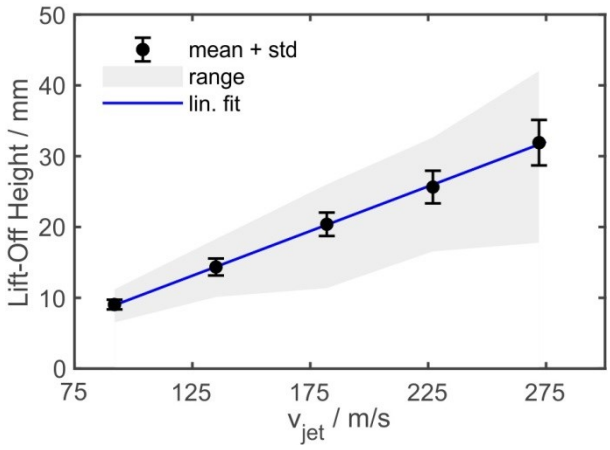

Figure 5. Dependence of the lift-off height on the jet exit velocity. The black closed symbols correspond to the mean lift-off height, the error bars correspond to the standard deviation. The grey shaded area corresponds to the range of measured lift-off heights and the blue curve is a linear fit through the mean values of the lift-off height.

As discussed in previous studies [11,17], the steady state jet flame in the DLR Jet-in-Hot-Coflow burner is, depending on the operating condition, partially stabilized by auto-ignition. One reason for the linear dependency of $\bar{h}_{LO}$ on v_{jet} is the dependence of h_{LO} on (a) the ignition delay time and (b) on turbulent flame propagation. When considering an auto-ignition stabilized flame, an igniting fluid element propagates further downstream within the ignition delay time at higher velocities. Additionally, the ignition delay time increases with increasing local strain rate [17], and therefore becomes longer for higher v_{jet}, since regions with higher strain rate are expected at the flame root. When considering turbulent flame propagation, flow velocities matching the flame propagation speed occur further downstream when increasing the jet exit velocity. The difference in flame stabilization and the flame stabilization mechanism regimes for the current configuration will be discussed in Section 3.4. Furthermore, turbulent mixing changes with v_{jet}, and can also influence the lift-off height.

3.2 Transient Fuel Injection and Auto-Ignition

In the following section, the influence of the boundary conditions on auto-ignition is discussed. To gain a better insight into the described phenomena, a typical image sequence of OH^* chemiluminescence showing the formation of an ignition kernel during the transient fuel injection is presented in Figure 6.

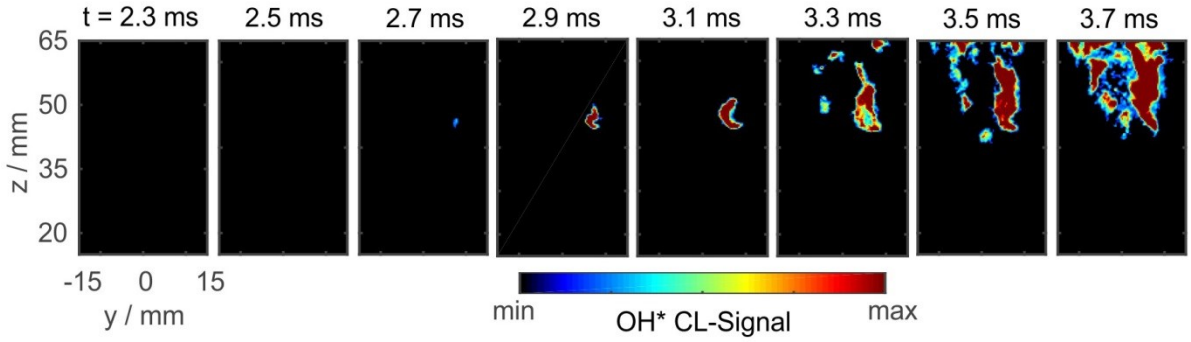

Figure 6. Time series of OH^* chemiluminescence of the formation of an ignition kernel during transient fuel injection for T_{cf} = 1501 K, v_{cf} = 4.1 m/s and v_{jet} = 182 m/s.

At t = 2.7 ms, an ignition kernel forms at z = 46 mm. After its formation, the ignition kernel growths mainly in axial and slightly in radial direction. At t = 3.3 ms, several additional ignition kernels are forming and eventually a closed reaction zone is seen.

Figure 7 shows the influence of the coflow temperature on the ignition time τ_{ign} and on the ignition height h_{ign}.

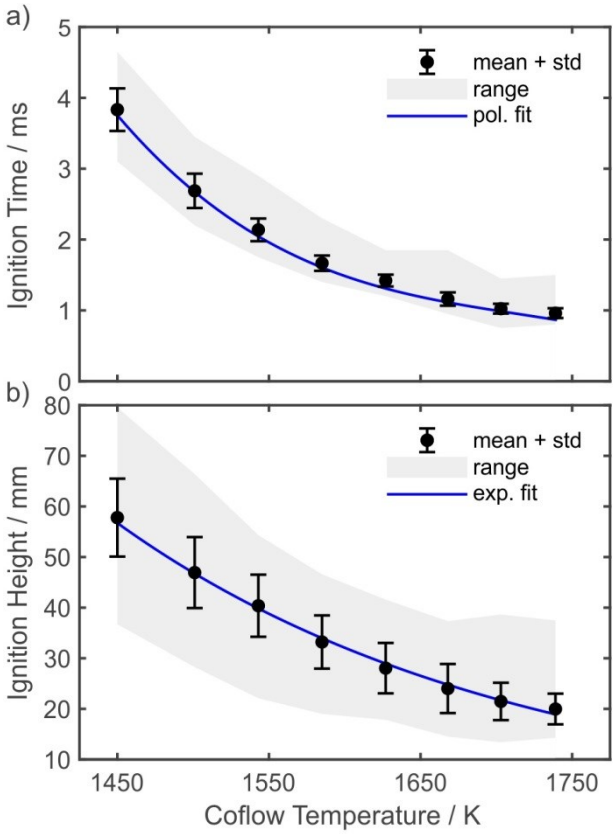

Figure 7. Dependence of a) ignition time and b) ignition height on the coflow temperature. The black closed symbols correspond to the mean measurement values, the error bars correspond to the standard deviation. The grey shaded area corresponds to the range of measurement values. The blue curve corresponds to a third-order polynomial fit (τ_{ign}), respectively an exponential fit (h_{ign}) and serves as guide to the eye.

Within the temperature range considered here, the mean ignition time $\bar{\tau}_{ign}$ varied between 3.83 ms (with $\sigma_{\tau_{ign}}$ = 0.3 ms) at T_{cf} = 1465 K and 0.96 ms (with $\sigma_{\tau_{ign}}$ = 0.07 ms) at T_{cf} = 1757 K and decreased, as expected, with increasing coflow temperature. While the absolute value of $\sigma_{\tau_{ign}}$ decreased with increasing coflow temperature, the relative standard deviation was constant at approximately 8% of $\bar{\tau}_{ign}$ for all operating conditions. For 1501 K < T_{cf} < 1543 K, the absolute sensitivity of the ignition time on T_{cf} was $S_{\bar{\tau}_{ign},T_{cf}}$ = 0.013 ms/K, and the relative sensitivity was $s_{\bar{\tau}_{ign},T_{cf}}$ = 8.26. For 1703 K < T_{cf} < 1739 K, the absolute sensitivity decreases to $S_{\bar{\tau}_{ign},T_{cf}}$ = 0.002 ms/K, and the relative sensitivity decreases to $s_{\bar{\tau}_{ign},T_{cf}}$ = 3.03.

A similar trend is observed for the mean ignition height $\bar{h}_{ign}$: with increasing coflow temperature, ignition kernels form at lower axial positions. For T_{cf} = 1450 K the mean ignition height was

$\bar{h}_{ign}$ = 57.79 mm (with $\sigma_{h_{ign}}$ = 7.70 mm), for T_{cf} = 1739 K, the mean ignition height was $\bar{h}_{ign}$ = 19.97 mm (with $\sigma_{h_{ign}}$ = 3.03 mm). The absolute value of the standard deviation decreases significantly with increasing coflow temperature, however the relative standard deviation increases slightly from 13% to 15%. The sensitivity of the ignition height is $S_{\bar{h}_{ign},T_{cf}}$ = 0.16 mm/K (or $s_{\bar{h}_{ign},T_{cf}}$ = 5.44) for 1501 K < T_{cf} < 1543 K and $S_{\bar{h}_{ign},T_{cf}}$ = 0.04 mm/K (or $s_{\bar{h}_{ign},T_{cf}}$ = 3.44) for 1703 K < T_{cf} < 1739 K. For the higher coflow temperatures, this sensitivity is similar to the temperature sensitivity of h_{LO}. However, for the colder coflow conditions, the temperature sensitivity of the ignition height is only half of the temperature sensitivity of the lift-off height.

Figure 8 shows the influence of the coflow velocity on the ignition time and ignition height. Since auto-ignition kernels form at very lean mixture fractions of about 1% of the stoichiometric mixture fraction [17], a clear influence of the coflow velocity on τ_{ign} and h_{ign} is expected, since regions where ignition kernels form are dominated by the coflow velocity.

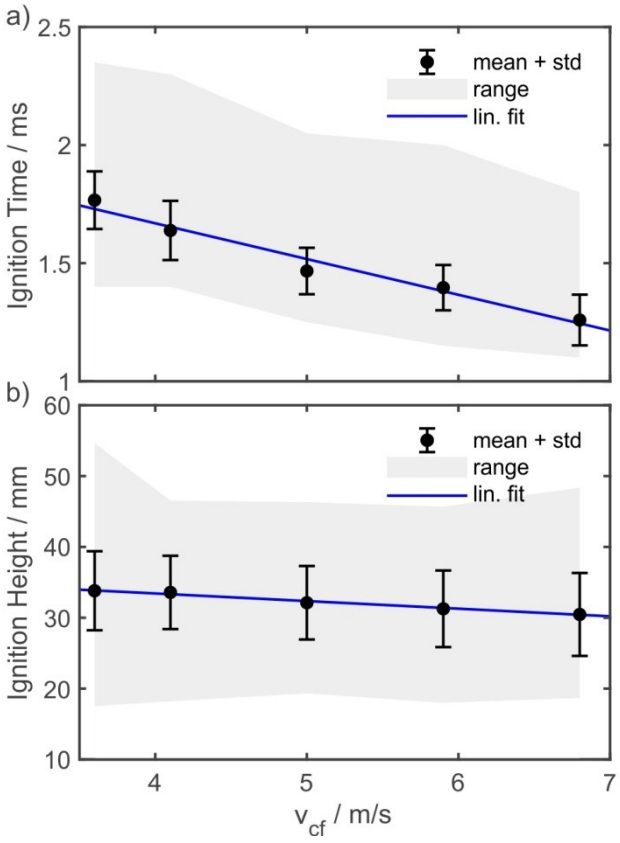

Figure 8. Dependence of a) ignition time and b) ignition height on the coflow velocity. The black closed symbols correspond to the mean measurement values, the error bars correspond to the standard deviation. The grey shaded area corresponds to the range of measurement values and the blue curve is a linear fit through the mean measurement values.

The ignition time decreased nearly linearly with increasing coflow velocity. While the mean ignition time at v_{cf} = 3.6 m/s is $\bar{\tau}_{ign}$ = 1.77 ms ($\sigma_{\tau_{ign}}$ = 0.12 ms), it decreased to $\bar{\tau}_{ign}$ = 1.26 ms ($\sigma_{\tau_{ign}}$ = 0.11 ms) at v_{cf} = 6.8 ms, corresponding to a relative sensitivity of $s_{\bar{\tau}_{ign},v_{cf}}$ = 0.55. The ignition height h_{ign} shows a similar trend: $\bar{h}_{ign}$ decreases with increasing coflow velocity from $\bar{h}_{ign}$ = 33.81 mm (with $\sigma_{h_{ign}}$ = 5.58 mm) at v_{cf} = 3.6 m/s to $\bar{h}_{ign}$ = 30.57 mm (with $\sigma_{h_{ign}}$ = 5.85 mm) at v_{cf} = 6.8 m/s. This corresponds to an absolute sensitivity of $S_{\bar{h}_{ign},v_{cf}}$ = 1.07 mm / m/s (or $s_{h_{ign},v_{cf}}$ = 0.17). Since the shear layer between the jet and the coflow becomes weaker with increasing coflow velocity, lower scalar dissipation rates are expected, and thus auto-ignition is less delayed by scalar dissipation at higher coflow velocities. Additionally, super-equilibrium OH that forms in the reaction zone of the matrix flame can be transported further downstream during its lifetime with increasing v_{cf}, and therefore can have an influence on the auto-ignition [44]. Furthermore, the thermal

power of the coflow increases with increasing coflow velocity and thus could influence auto-ignition, for example due to heating of the fuel nozzle and thus slight preheating of the fuel or due to radiation effects.

The dependence of the axial location of the lowest ignition kernel on the jet fuel mass flow in the Delft Jet-in-Hot coflow burner was reported by Oldenhof et al. [15,20] (for steady state fuel injection). They found that ignition kernels form closer to the fuel nozzle with increasing jet velocity. A similar trend was observed for the lift-off height in the Delft JHC [15] and was attributed to the positive radial temperature gradient of the coflow and entrainment of ambient air for higher coflow velocities.

To further assess the possible influence of an increased OH mole fraction X_{OH} in the coflow at higher coflow velocities on the ignition delay time τ_{ign}, chemical kinetic calculations of the ignition delay time for different OH mole fractions in the coflow were performed using Chemical Workbench [45] and the GRI 3.0 mechanism [42]. The dependence of τ_{ign} on X_{OH} is shown in Figure 9 for a coflow temperature of T_{cf} = 1585 K (ϕ_{cf} = 0.506).

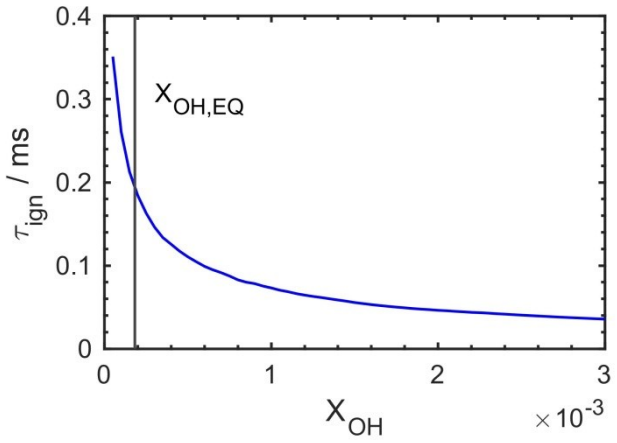

Figure 9. Dependence of the chemical kinetic ignition delay time on the OH mole fraction in the coflow.

The solid blue line corresponds to the calculated ignition delay time, the vertical black line corresponds to the equilibrium OH concentration for the measured coflow temperature. It is evident that τ_{ign} is very sensitive on X_{OH}. In atmospheric pressure flames, the life-time of super-equilibrium OH is on the order of several milliseconds (e.g., for methane/air flames see [46]). Thus, super-equilibrium OH transported downstream could be an explanation for the observed decreasing ignition

time with increasing coflow velocity, which probably cannot be explained based on fluid dynamic aspects alone.

Last, the influence of the jet exit velocity on the auto-ignition is discussed. Figure 10 shows the influence of v_{jet} on h_{ign} and τ_{ign}.

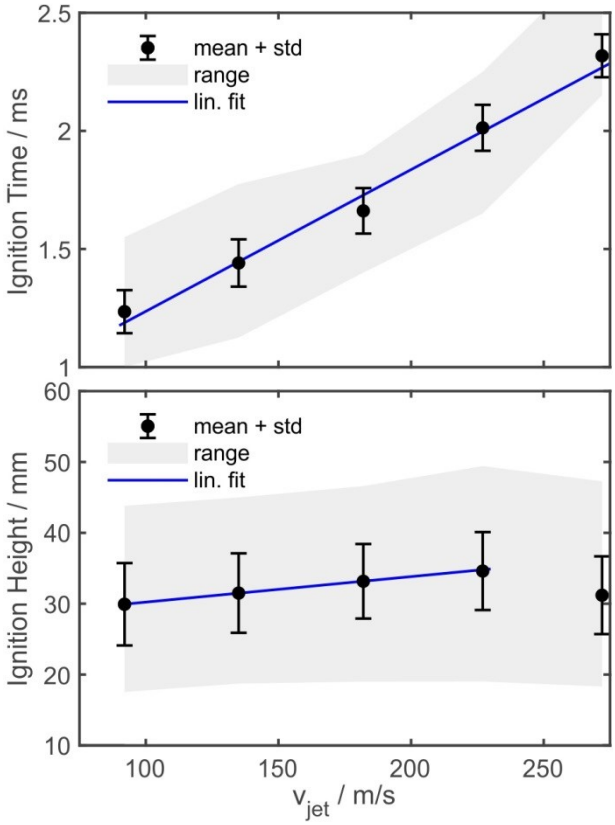

Figure 10. Dependence of a) ignition time and b) ignition height on the jet exit velocity. The black closed symbols correspond to the mean measurement values, the error bars correspond to the standard deviation. The grey shaded area corresponds to the range of measurement values and the blue curve is a linear fit through the mean measurement values.

The ignition time increases almost linearly with increasing v_{jet}, the absolute sensitivity of the ignition time to v_{jet} is $S_{\bar{\tau}_{ign},v_{jet}}$ = 0.006 ms / m/s, the relative sensitivity is $s_{\bar{\tau}_{ign},v_{jet}}$ = 0.60. For v_{jet} < 250 m/s, the ignition height also increases linearly with increasing v_{jet}. However, for v_{jet} > 250 m/s, the trend is inverted and $\bar{h}_{ign}$ decreases with increasing v_{jet}. In the linear regime, the absolute sensitivity of $\bar{h}_{ign}$ to v_{jet} is $S_{\bar{h}_{ign},v_{jet}}$ = 0.036 mm / m/s, the relative sensitivity is $s_{\bar{h}_{ign},v_{jet}}$ = 0.18. The sensitivity of

$\bar{h}_{ign}$ to the jet exit velocity is almost a factor of 5 lower than the sensitivity of $\bar{h}_{LO}$ to v_{jet}. However, the inversion of the trend, as observed for auto-ignition, was not observed for the steady state jet flame. With DNS calculations, Hilbert et al. [47] have shown that ignition is mainly influenced by the occurrence of a minimal scalar dissipation rate, and is less influenced by turbulence or the Reynolds-number. The minimal value of the scalar dissipation rate, where ignition can occur, is only mildly dependent on the turbulence intensity [47]. The ignition height is less influenced by turbulence, but more by the residence time of an igniting fluid parcel, which leads to higher ignition heights with increasing velocities for the same residence time.

3.3 Relative and Absolute Sensitivities on Boundary Conditions

Figure 11 summarizes the relative sensitivities of $\bar{h}_{LO}$, $\bar{h}_{ign}$ and $\bar{\tau}_{ign}$ on the examined boundary conditions, namely v_{jet}, v_{cf} and T_{cf}.

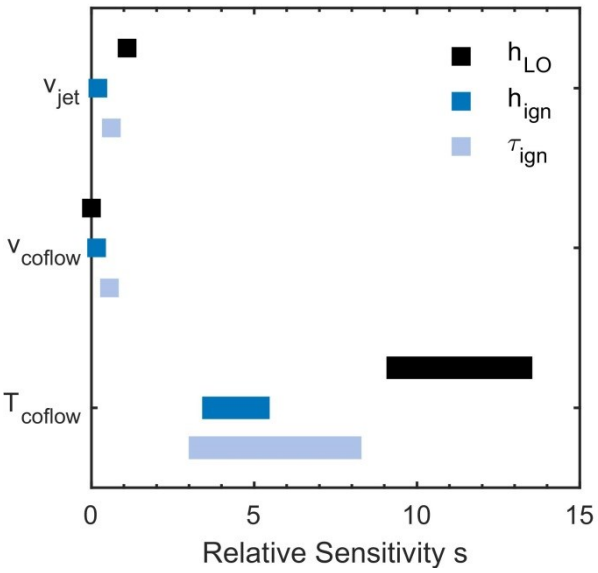

Figure 11. Relative sensitivities s of lift-off height $\bar{h}_{LO}$, ignition height $\bar{h}_{ign}$ and ignition time $\bar{\tau}_{ign}$ on the boundary conditions.

The variation of v_{jet} had a considerably larger influence on $\bar{h}_{LO}$ in comparison to $\bar{h}_{ign}$. Auto-ignition assisted flame propagation has a large influence on the stabilization of the steady state flame, depending on the operating condition, as will be discussed below. Therefore, $\bar{h}_{LO}$ increases with increasing v_{jet} due to the higher fluid velocity in which the flame is stabilized, similar to jet flames in a cold coflow. The maximum flame speeds occur near the stoichiometric mixture fraction ξ_{st}, auto-ignition occurs at the so-called most reactive mixture fraction ξ_{mr} [28], which is about 1% of ξ_{st} for the current conditions [17]. Therefore, $\bar{h}_{LO}$ is more influenced by a change of v_{jet} than h_{ign}. In contrast, auto-ignition occurs in areas which are dominated by the coflow velocity. Here, no significant influence of v_{cf} on $\bar{h}_{LO}$ was observed, but both $\bar{h}_{ign}$ and $\bar{\tau}_{ign}$ were influenced by v_{cf}.

T_{cf} had the largest influence, the relative sensitivity of all system response quantities on T_{cf} was almost one order of magnitude higher than on v_{jet} or v_{cf}. Since all measured quantities had a non-linear dependence on T_{cf}, the horizontal bars in Figure 11 correspond to the range of the relative

sensitivity for T_{cf}. $\bar{h}_{LO}$ showed the highest variance of the relative sensitivity s; here, s for the lower coflow temperatures is almost three times higher than at higher coflow temperatures. The lowest relative sensitivity on T_{cf} was observed for the ignition height. A possible explanation for this observation is the strong influence of strain and scalar dissipation on auto-ignition sites. Auto-ignition can only occur at strain rates below the critical strain rate [17], and the scalar dissipation decreases strongly with increasing axial position [24]. Therefore it is possible that auto-ignition is suppressed upstream of a certain axial position. Downstream of this position, the scalar dissipation rate drops quickly [24], and hence the axial position of the auto-ignition is less influenced by T_{cf} and more strongly influenced by favorable flow structures with sufficient low scalar dissipation rates, as observed in previous studies [17,24]. The ignition time shows a great variance of the relative sensitivity. This is due to the strong dependence of τ_{ign} on the temperature.

The formation of ignition kernels is strongly influenced by the occurrence of favorable flow structures with low scalar dissipation rates. Such structures are apparently only mildly influenced by v_{jet} and seem to appear at similar heights, independent of v_{jet}. The ignition time is much more sensitive on a change of v_{jet} than the ignition height. This could be explained by a decelerating influence of high scalar dissipation rates on the auto-ignition at higher v_{jet}.

A similar trend is observable when comparing the absolute sensitivities S of the lift-off height and the ignition height with respect to the velocity boundary conditions, as shown in Figure 12.

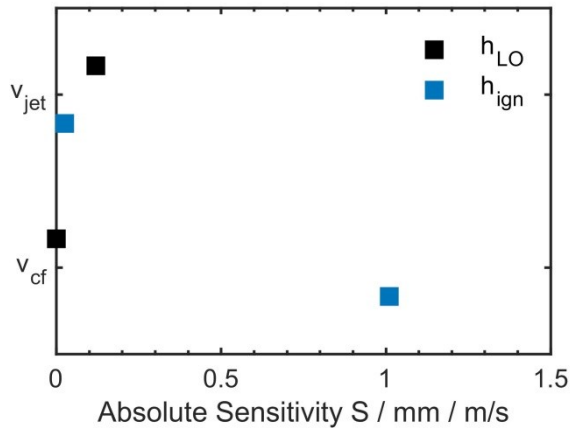

Figure 12. Absolute sensitivities S of the lift-off height $\bar{h}_{LO}$ and the ignition height $\bar{h}_{ign}$ on the velocity boundary conditions v_{cf} and v_{jet}.

The lift-off height shows a clear sensitivity to the jet velocity, while it is not influenced by the coflow velocity. The influence of the jet velocity on the lift-off height is considerably higher than on the ignition height, which is due to the flame stabilization mechanism and the trend of the flame to anchor near the stoichiometric mixture fraction, while auto-ignition occurs at very lean mixtures. Hence, the sensitivity of the ignition height with respect to the coflow velocity is almost an order of magnitude higher than on the jet velocity.

3.4 Influence of Boundary Conditions on the Flame Stabilization Mechanism

As evident from the discussion in Sec. 3.1 and 3.2 (cf. Figure 5 Figure 10), the mean auto-ignition height is typically downstream of the mean flame stabilization height. This is due to several reasons. An auto-ignition event that eventually leads to a steady state flame can be described by three steps: (1) formation of an auto-ignition kernel at a given height (2) subsequent expansion of the ignition kernel upstream and downstream and (3) establishment of a stably burning lifted jet flame. Hence, the mean ignition height is typically downstream of the mean stabilization height. Additionally, ignition kernels occur over a broader range of axial locations than the lift-off height. Thus, statistically ignition kernels can also occur below the mean flame base. This is illustrated by the probability density functions (PDFs) of the lift-off height and the auto-ignition height for T_{cf} = 1500 K, v_{cf} = 4.1 m/s and v_{jet} = 182 m/s, as shown in Figure 13.

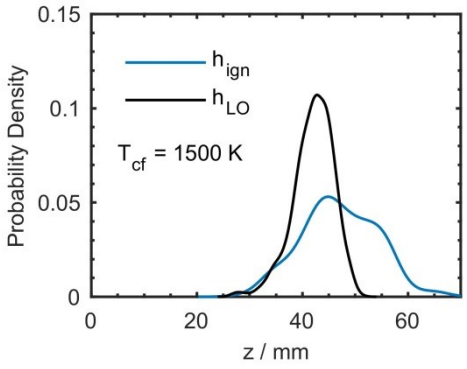

Figure 13. Probability density functions (PDFs) of the ignition height h_{ign} (blue curve) and lift-off height h_{LO} (black curve) for T_{cf} = 1500 K, v_{cf} = 4.1 m/s and v_{jet} = 182 m/s.

Here, the PDFs of the ignition height h_{ign} and lift-off height h_{LO} overlap at lower axial regions, but the maximum and distribution of the PDF for the ignition height is further downstream in comparison to the lift-off height. This is evident for a stabilization of the lifted flame by auto-ignition in this temperature range, since ignition kernels can occur in the range of the flame base

At higher coflow temperatures, the behavior of the lift-off height and the ignition height is different. Figure 14 shows the PDFs of the ignition height h_{ign} and the lift-off height h_{LO} for a coflow temperature of 1739 K.

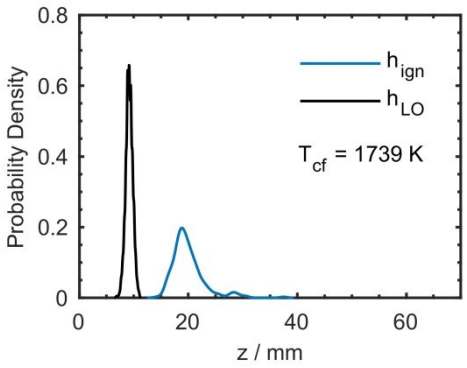

Figure 14. Probability density functions (PDFs) of the ignition height h_{ign} (blue curve) and lift-off height h_{LO} (black curve) for T_{cf} = 1739 K, v_{cf} = 4.1 m/s and v_{jet} = 182 m/s.

Here, the PDFs of the two SRQs shift further apart, and ignition kernels only occur downstream of the flame stabilization zone. Thus, for T_{cf} = 1739 K, the flame is probably not stabilized by auto-ignition. Instead, the flame stabilization mechanism seems to switch from auto-ignition stabilized to flame propagation stabilized with increasing coflow temperatures. Consequently, auto-ignition kernels forming below the flame base are not observed in this temperature range.

This leads to the conclusion that the flame stabilization mechanism in the current flow and temperature regime is a competition between auto-ignition and flame propagation. Close to the fuel nozzle, high scalar dissipation rates and strain rates occur. High strain rates are known to delay or hinder auto-ignition under the current conditions [17]. Thus, auto-ignition is only possible downstream of a critical ignition height, where the local strain rate falls below a critical strain rate, above which no auto-ignition can occur [24]. Flame propagation on the other hand is less sensitive to strain and scalar dissipation than auto-ignition, and thus the flame stabilization regime changes for certain conditions from auto-ignition stabilized to flame-propagation stabilized. To further assess this point, chemical kinetic calculations of the extinction strain rate k_{ext} (at which an already established flame extinguishes) and of the critical strain rate k_{crit} (above which no auto-ignition is possible) were performed as described in Section 2.5. Figure 15 shows the calculated critical strain rate and extinction strain rate for the coflow conditions studied in the current experiment.

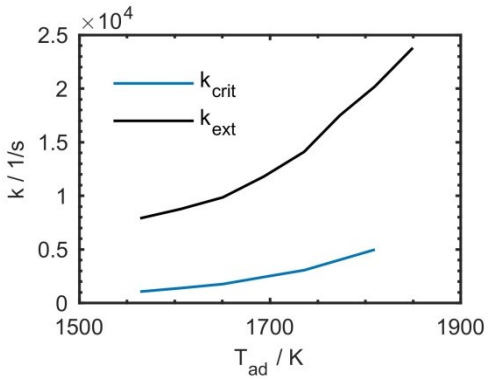

Figure 15 Extinction strain rate k_{ext} and critical strain rate k_{crit} for the boundary conditions of the current experiment.

The extinction strain rate for the conditions of the current experiment is approximately three to eight times higher than the critical strain rate, depending on the coflow conditions. Hence, a flame can stabilize at higher strain rates and thus further upstream than auto-ignition can occur. However, also the flame speed has to be high enough for the flame to propagate to high strain rate regions further upstream. From the literature, it is known that maximum flame speeds occur near the stoichiometric mixture fraction [48], even for conditions with cold fuel and hot oxidizer, where the mixture temperature decreases with increasing mixture fraction [39]. Additionally, the laminar flame speed increases with increasing strain rate [49,50]. Combining these factors leads to the conclusion that for certain boundary conditions, auto-ignition can occur below the flame base and contribute to the flame stabilization, while for other boundary conditions, the flame can propagate further downstream due to the lesser sensitivity to the strain rate. Here, auto-ignition is hindered by the critical strain rate and can only occur at locations downstream of the mean flame stabilization height.

When taking a closer look on the statistical distribution of the lift-off height h_{LO} and the ignition height h_{ign}, different flame stabilization regimes can also be observed for different jet exit velocities. Figure 16 shows PDFs of h_{LO} and h_{ign} for jet exit velocities v_{jet} = 92 m/s and v_{jet} = 227 m/s.

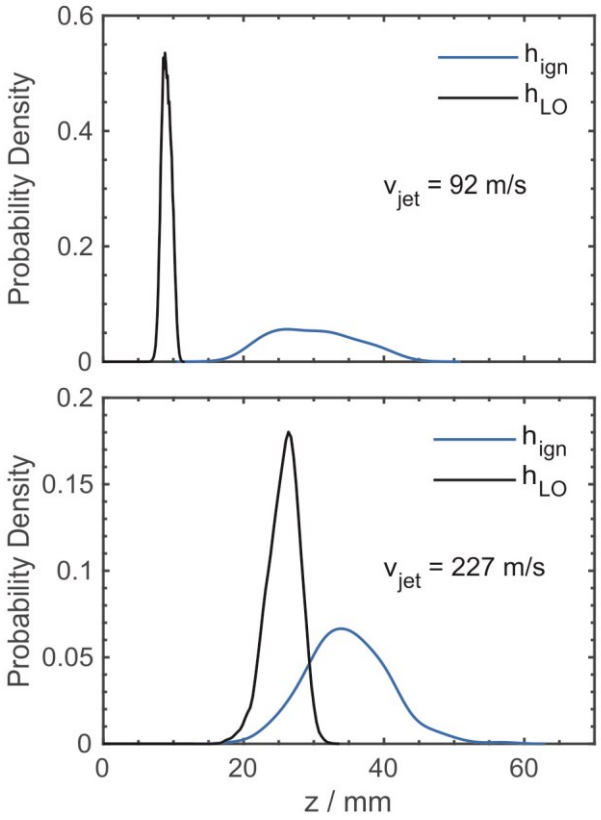

Figure 16. Probability density functions of the ignition height (blue curves) and lift-off height (black curves) for jet exit velocities of v_{jet} = 92 m/s and v_{jet} = 227 m/s (at T_{cf} = 1585 K and v_{cf} = 4.1 m/s).

At v_{jet} = 92 m/s, auto-ignition occurs downstream of the flame stabilization zone, since the flame anchors close to the nozzle due to the moderately high flow velocities occurring here. Consequently, auto-ignition is not possible close to the nozzle due to the high strain rates occurring here; in previous experiments in the same configurations, a laminar-like phase with very high mixture fraction gradients was observed close to the nozzle [11,24]. When increasing the jet exit velocity to v_{jet} = 227 m/s, the distribution of the lift-off height and the ignition height changes. The regions of the formation of ignition kernels and the flame stabilization partially overlap. The steady-state lift-off height increases with increasing jet exit velocity. Similarly, regions with adequate flow velocities near the stoichiometric mixture fraction, where the maximum flame speeds occur, are shifted further downstream. Auto-ignition occurs at very lean mixture fractions, and thus is less influenced by the jet velocity and more by the occurrence of flow structures favorable for auto-ignition (i.e. low strain and scalar dissipation rates). Close to the nozzle, the strain rate is above the critical strain rates, and thus

no ignition is possible here, regardless of the jet exit velocity. This is also supported by the range of observed ignition heights in Figure 10. Here, the minimal ignition height for all studied jet exit velocities is > 20 mm, thus supporting the thesis of auto-ignition occurring only downstream of a region of very high strain rates. Downstream of this region, auto-ignition can occur, and those regions do not seem to change much in axial location with a variation of the jet exit velocity.

4 Summary and Conclusions

The influence of boundary conditions on flame stabilization and auto-ignition in the DLR Jet-in-Hot-Coflow burner was studied using high-speed OH* chemiluminescence imaging and chemical kinetic calculations. The coflow temperature, as well as the coflow and jet velocities were varied over a broad range, and their influence on different system response quantities (SRQs), namely the flame lift-off height (for steady-state fuel injection) and the height and time of the initial auto-ignition kernel (for transient fuel injection) was measured. To quantify and compare the influence of different boundary conditions a relative sensitivity was defined. Increasing the jet velocity led to a linear increase of all SRQs. The lift-off height of the steady state jet flame showed the largest sensitivity because the flame stabilization mechanism is a combination of auto-ignition and flame propagation. The coflow velocity had no measurable influence on the lift-off height; however, auto-ignition kernels were mildly influence by the coflow velocity. Since auto-ignition kernels under the current conditions form at extremely low mixture fractions, igniting fluid parcels are influenced by the coflow velocity. All SRQs showed a high temperature sensitivity. However, steady state jet flame and auto-ignition showed different relative sensitivities to the coflow temperature. This was attributed to a stronger influence of the local strain rate on the formation of auto-ignition kernels in contrast to the flame stabilization.

Probability density functions of the ignition height and the flame lift-off height showed that different flame stabilization mechanisms are observed, depending on the coflow temperature and the jet exit velocity. For lower coflow temperatures and higher jet exit velocities, the PDFs of the ignition height and the lift-off height overlapped at lower axial locations, indicating that auto-ignition is a key contributor to the flame stabilization mechanism in those regimes. For higher coflow temperatures and lower jet exit velocities, the PDFs of the ignition height and the lift-off height did not overlap, leading to the conclusion that flame propagation is the dominant contributor to the flame stabilization mechanism. Chemical kinetic calculations of the critical strain rate, above which no auto-ignition can occur, and the extinction strain rate, above which an already established flame extinguishes, further supported those conclusions, since the extinction strain rate is a factor of 3 to 8 higher as the critical strain rate. Furthermore, an increase in the local strain rate leads to longer ignition delay times, but to

higher flame propagation velocities. Thus, a flame can survive at lower axial locations and at higher strain rates in comparison to auto-ignition kernels.

The presented results are important for the uncertainty quantification of numerical models. Here, especially the precision (and variance) of the coflow temperature has to be considered. Future work will involve the assessment of the quality of large-eddy simulations of the current test case using the validation data provided here.

Acknowledgements

Robert Schießl is gratefully acknowledged for performing the INSFLA simulations. Juliane Prause is gratefully acknowledged for the fruitful discussions.

Conflict of Interest

The authors declare that they have no conflict of interest.

References

1. Güthe, F., Hellat, J., Flohr, P.: The Reheat Concept: The Proven Pathway to Ultralow Emissions and High Efficiency and Flexibility. J. Eng. Gas Turbines Power **131**(2), 021503 (2009). doi:10.1115/1.2836613
2. Fleck, J.M., Griebel, P., Steinberg, A.M., Arndt, C.M., Aigner, M.: Auto-ignition and flame stabilization of hydrogen/natural gas/nitrogen jets in a vitiated cross-flow at elevated pressure. Int. J. Hydrogen Energy **38**(36), 16441-16452 (2013). doi:10.1016/j.ijhydene.2013.09.137
3. Fleck, J.M., Griebel, P., Steinberg, A.M., Arndt, C.M., Naumann, C., Aigner, M.: Autoignition of hydrogen/nitrogen jets in vitiated air crossflows at different pressures. Proc. Combust. Inst. **34**(2), 3185-3192 (2013). doi:10.1016/j.proci.2012.05.039
4. Lammel, O., Schütz, H., Schmitz, G., Lückerath, R., Stöhr, M., Noll, B., Aigner, M., Hase, M., Krebs, W.: FLOX® Combustion at High Power Density and High Flame Temperatures. J. Eng. Gas Turbines Power **132**(12), 121503 (2010). doi:10.1115/1.4001825
5. Lammel, O., Stöhr, M., Kutne, P., Dem, C., Meier, W., Aigner, M.: Experimental Analysis of Confined Jet Flames by Laser Measurement Techniques. J. Eng. Gas Turbines Power **134**(4), 041506 (2012). doi:10.1115/1.4004733
6. Boxx, I., Arndt, C.M., Carter, C.D., Meier, W.: Highspeed Laser Diagnostics for the Study of Flame Dynamics in a Lean Premixed Gas Turbine Model Combustor. Exp. Fluids **52**(3), 555-567 (2012). doi:10.1007/s00348-010-1022-x
7. Cabra, R., Myhrvold, T., Chen, J.Y., Dibble, R.W., Karpetis, A.N., Barlow, R.S.: Simultaneous Laser Raman-Rayleigh-LIF Measurements and Numerical Modeling Results of a Lifted Turbulent H_2/N_2 Jet Flame in a Vitiated Coflow. Proc. Combust. Inst. **29**(2), 1881-1888 (2002). doi:10.1016/S1540-7489(02)80228-0
8. Dally, B.B., Karpetis, A.N., Barlow, R.S.: Structure of turbulent non-premixed jet flames in a diluted hot coflow. Proc. Combust. Inst. **29**(1), 1147-1154 (2002). doi:10.1016/S1540-7489(02)80145-6
9. Medwell, P.R., Kalt, P.A.M., Dally, B.B.: Imaging of Diluted Turbulent Ethylene Flames Stabilized on a Jet in Hot Coflow (JHC) Burner. Combust. Flame **152**(1-2), 100-113 (2008). doi:10.1016/j.combustflame.2007.09.003
10. Gordon, R.L., Masri, A.R., Mastorakos, E.: Simultaneous Rayleigh temperature, OH- and CH_2O-LIF imaging of methane jets in a vitiated coflow. Combust. Flame **155**(1-2), 181-195 (2008). doi:10.1016/j.combustflame.2008.07.001
11. Arndt, C.M., Gounder, J.D., Meier, W., Aigner, M.: Auto-ignition and flame stabilization of pulsed methane jets in a hot vitiated coflow studied with high-speed laser and imaging techniques. Appl. Phys. B **108**(2), 407-417 (2012). doi:10.1007/s00340-012-4945-5
12. Johannessen, B., North, A., Dibble, R., Lovas, T.: Experimental studies of autoignition events in unsteady hydrogen-air flames. Combust. Flame **162**(9), 3210-3219 (2015). doi:10.1016/j.combustflame.2015.05.008
13. Macfarlane, A.R.W., Dunn, M.J., Juddoo, M., Masri, A.R.: Stabilisation of turbulent auto-igniting dimethyl ether jet flames issuing into a hot vitiated coflow. Proc. Combust. Inst. **36**(2), 1661-1668 (2017). doi:https://doi.org/10.1016/j.proci.2016.08.028
14. Cabra, R., Chen, J.Y., Dibble, R.W., Karpetis, A.N., Barlow, R.S.: Lifted methane-air jet flames in a vitiated coflow. Combust. Flame **143**(4), 491-506 (2005). doi:10.1016/j.combustflame.2005.08.019
15. Oldenhof, E., Tummers, M.J., van Veen, E.H., Roekaerts, D.J.E.M.: Ignition kernel formation and lift-off behaviour of jet-in-hot-coflow flames. Combust. Flame **157**(6), 1167-1178 (2010). doi:10.1016/j.combustflame.2010.01.002
16. Medwell, P.R., Dally, B.B.: Experimental Observation of Lifted Flames in a Heated and Diluted Coflow. Energy Fuels **26**(9), 5519-5527 (2012). doi:10.1021/ef301029u

17. Arndt, C.M., Schießl, R., Gounder, J.D., Meier, W., Aigner, M.: Flame stabilization and auto-ignition of pulsed methane jets in a hot coflow: Influence of temperature. Proc. Combust. Inst. **34**(1), 1483-1490 (2013). doi:10.1016/j.proci.2012.05.082
18. Eitel, F., Pareja, J., Geyer, D., Johchi, A., Michel, F., Elsäßer, W., Dreizler, A.: A novel plasma test rig for auto-ignition studies of turbulent non-premixed flows. Exp. Fluids **56**, 186 (2015). doi:10.1007/s00348-015-2059-7
19. Evans, M.J., Medwell, P.R., Wu, H., Stagni, A., Ihme, M.: Classification and lift-off height prediction of non-premixed MILD and autoignitive flames. Proc. Combust. Inst. **36**(3), 4297-4304 (2017). doi:https://doi.org/10.1016/j.proci.2016.06.013
20. Oldenhof, E., Tummers, M.J., van Veen, E.H., Roekaerts, D.J.E.M.: Role of entrainment in the stabilisation of jet-in-hot-coflow flames. Combust. Flame **158**(8), 1553-1563 (2011). doi:10.1016/j.combustflame.2010.12.018
21. Papageorge, M.J., Arndt, C., Fuest, F., Meier, W., Sutton, J.A.: High-speed mixture fraction and temperature imaging of pulsed, turbulent fuel jets auto-igniting in high-temperature, vitiated co-flows. Exp. Fluids **55**(7), 1763 (2014). doi:10.1007/S00348-014-1763-Z
22. Meier, W., Boxx, I., Arndt, C., Gamba, M., Clemens, N.: Investigation of Auto-Ignition of a Pulsed Methane Jet in Vitiated Air Using High-Speed Imaging Techniques. J. Eng. Gas Turbines Power **133**(2), 021504 (2011). doi:10.1115/1.4002014
23. Oldenhof, E., Tummers, M.J., van Veen, E.H., Roekaerts, D.J.E.M.: Transient response of the Delft jet-in-hot coflow flames. Combust. Flame **159**(2), 697-706 (2012). doi:10.1016/j.combustflame.2011.08.001
24. Arndt, C.M., Papageorge, M.J., Fuest, F., Sutton, J.A., Meier, W., Aigner, M.: The role of temperature, mixture fraction, and scalar dissipation rate on transient methane injection and auto-ignition in a jet in hot coflow burner. Combust. Flame **167**, 60-71 (2016). doi:10.1016/j.combustflame.2016.02.027
25. Eitel, F., Pareja, J., Johchi, A., Böhm, B., Geyer, D., Dreizler, A.: Temporal evolution of auto-ignition of ethylene and methane jets propagating into a turbulent hot air co-flow vitiated with NOx. Combust. Flame **177**, 193-206 (2017). doi:10.1016/j.combustflame.2016.12.009
26. Pareja, J., Johchi, A., Li, T., Dreizler, A., Böhm, B.: A study of the spatial and temporal evolution of auto-ignition kernels using time-resolved tomographic OH-LIF. Proc. Combust. Inst. (2018). doi:https://doi.org/10.1016/j.proci.2018.06.028
27. Arndt, C.M., Papageorge, M.J., Fuest, F., Sutton, J.A., Meier, W.: Experimental Investigation of the Auto-Ignition of a Transient Propane Jet-in-Hot-Coflow. Proc. Combust. Inst. (2018). doi:10.1016/j.proci.2018.06.195
28. Mastorakos, E.: Ignition of Turbulent Non-Premixed Flames. Prog. Energy Combust. Sci. **35**(1), 57-97 (2009). doi:10.1016/j.pecs.2008.07.002
29. Myhrvold, T., Ertesvag, I.S., Gran, I.R., Cabra, R.: A Numerical Investigation of a Lifted H_2/N_2 Turbulent Jet Flame in a Vitiated Coflow. Combustion Science and Technology **178**(6), 1001-1030 (2006). doi:10.1080/00102200500270106
30. De, A., Oldenhof, E., Sathiah, P., Roekaerts, D.: Numerical Simulation of Delft-Jet-in-Hot-Coflow (DJHC) Flames Using the Eddy Dissipation Concept Model for Turbulence–Chemistry Interaction. Flow, Turbulence and Combustion **87**(4), 537-567 (2011). doi:10.1007/s10494-011-9337-0
31. Masri, A.R., Cao, R., Pope, S.B., Goldin, G.M.: PDF calculations of turbulent lifted flames of H_2/N_2 fuel issuing into a vitiated co-flow. Combustion Theory and Modelling **8**(1), 1-22 (2004). doi:10.1088/1364-7830/8/1/001
32. Gordon, R.L., Masri, A.R., Pope, S.B., Goldin, G.M.: A numerical study of auto-ignition in turbulent lifted flames issuing into a vitiated co-flow. Combustion Theory and Modelling **11**(3), 351-376 (2007). doi:10.1080/13647830600903472
33. Navarro-Martinez, S., Kronenburg, A.: LES-CMC simulations of a lifted methane flame. Proceedings of the ASME Turbo Expo **32**(1), 1509-1516 (2009). doi:10.1016/j.proci.2008.06.178

34. Duwig, C., Fuchs, L.: Large Eddy Simulation of a H_2/N_2 Lifted Flame in a Vitiated Co-Flow. Combustion Science and Technology **180**(3), 453-480 (2008). doi:10.1080/00102200701741327
35. Schulz, O., Jaravel, T., Poinsot, T., Cuenot, B., Noiray, N.: A criterion to distinguish autoignition and propagation applied to a lifted methane–air jet flame. Proc. Combust. Inst. **36**(2), 1637-1644 (2017). doi:https://doi.org/10.1016/j.proci.2016.08.022
36. Roy, C., Oberkampf, W.: A Complete Framework for Verification, Validation, and Uncertainty Quantification in Scientific Computing. In: 48th AIAA Aerospace Sciences Meeting 2010
37. Chris Morley. Gaseq - A chemical equilibrium program for windows. Version 0.79 (2005). http://www.gaseq.co.uk/
38. Prucker, S., Meier, W., Stricker, W.: A flat flame burner as calibration source for combustion research: Temperatures and species concentrations of premixed H_2/air flames. Rev. Sci. Instrum. **65**(9), 2908-2911 (1994). doi:10.1063/1.1144637
39. Arndt, C.M.: Entwicklung und Anwendung von Hochgeschwindigkeits-Lasermesstechnik zur Untersuchung von Selbstzündung. Dissertation, Universität Stuttgart (2017)
40. David G. Goodwin, Harry K. Moffat, and Raymond L. Speth. Cantera: An object-oriented software toolkit for chemical kinetics, thermodynamics, and transport processes. Version 2.4.0 (2018) https://www.cantera.org
41. Fiala, T., Sattelmayer, T.: Nonpremixed Counterflow Flames: Scaling Rules for Batch Simulations. Journal of Combustion **2014**, Article ID 484372 (2014). doi:10.1155/2014/484372
42. Smith, G.P., Golden, D.M., Frenklach, M., Moriarty, N.W., Eiteneer, B., Goldenberg, M., Bowman, C.T., Hanson, R.K., Song, S., William C. Gardiner, J., Lissianski, V.V., Qin, Z.: GRI 3.0. http://www.me.berkeley.edu/gri_mech/.
43. Stahl, G., Warnatz, J.: Numerical investigation of time-dependent properties and extinction of strained methane- and propane-air flamelets. Combust. Flame **85**(3-4), 285-299 (1991). doi:10.1016/0010-2180(91)90134-W
44. Gerlinger, P., Nold, K., Aigner, M.: Influence of reaction mechanisms, grid spacing, and inflow conditions on the numerical simulation of lifted supersonic flames. International Journal for Numerical Methods in Fluids **62**(12), 1357-1380 (2010). doi:10.1002/fld.2076
45. KintechLab. Chemical Workbench 4.1. (2014)
46. Sadanandan, R., Stöhr, M., Meier, W.: Simultaneous OH-PLIF and PIV measurements in a gas turbine model combustor. Appl. Phys. B **90**(3-4), 609-618 (2008). doi:10.1007/s00340-007-2928-8
47. Hilbert, R., Thévenin, D.: Autoignition of turbulent non-premixed flames investigated using direct numerical simulation. Combust. Flame **128**(1-2), 22-37 (2002). doi:10.1016/S0010-2180(01)00330-3
48. Warnatz, J., Maas, U., Dibble, R.W.: Combustion - Physical and Chemical Fundamentals, Modeling und Simulation, Experiments, Pollutant Formation, 4th ed. Springer Verlag, Berlin (2006)
49. Foley, C.W., Chterev, I., Seitzman, J., Lieuwen, T.: High Resolution Particle Image Velocimetry and CH-PLIF Measurements and Analysis of a Shear Layer Stabilized Flame. J. Eng. Gas Turbines Power **138**(3), 031603-031603-031613 (2015). doi:10.1115/1.4031367
50. Foley, C., Chterev, I., Noble, B., Seitzman, J., Lieuwen, T.: Shear layer flame stabilization sensitivities in a swirling flow. International Journal of Spray and Combustion Dynamics **9**(1), 3-18 (2016). doi:10.1177/1756827716653426